Title

Plant Virus Intratumoral Immunotherapy with CPMV and PVX Elicits Durable Antitumor Immunity in a Mouse Model of Diffuse Large B–Cell Lymphoma

Journal

Molecular Pharmaceutics, 21(12)

ISSN

1543-8384

Authors

de Oliveira, Jessica Fernanda Affonso

Moreno-Gonzalez, Miguel A

Ma, Yifeng

et al.

Publication Date

2024-12-02

DOI

10.1021/acs.molpharmaceut.4c00507

Peer reviewed

HHS Public Access

Author manuscript

Mol Pharm. Author manuscript; available in PMC 2024 December 20.

Published in final edited form as:

Mol Pharm. 2024 December 02; 21(12): 6206–6219. doi:10.1021/acs.molpharmaceut.4c00507.

Plant Virus Intratumoral Immunotherapy with CPMV and PVX Elicits Durable Antitumor Immunity in a Mouse Model of Diffuse Large B-Cell Lymphoma

Jessica Fernanda Affonso de Oliveira[‡],

Aiiso Yufeng Li Family Department of Chemical and Nano Engineering, University of California San Diego, La Jolla, California 92093, United States; Shu and K.C. Chien and Peter Farrell Collaboratory, University of California San Diego, San Diego, California 92093, United States; Center for Nano-ImmunoEngineering and Moores Cancer Center, University of California San Diego, La Jolla, California 92093, United States

Miguel A. Moreno-Gonzalez[‡],

Aiiso Yufeng Li Family Department of Chemical and Nano Engineering, University of California San Diego, La Jolla, California 92093, United States; Shu and K.C. Chien and Peter Farrell Collaboratory, University of California San Diego, San Diego, California 92093, United States; Center for Nano-ImmunoEngineering and Moores Cancer Center, University of California San Diego, La Jolla, California 92093, United States

Yifeng Ma,

Aiiso Yufeng Li Family Department of Chemical and Nano Engineering, University of California San Diego, La Jolla, California 92093, United States; Shu and K.C. Chien and Peter Farrell Collaboratory, University of California San Diego, San Diego, California 92093, United States; Center for Nano-ImmunoEngineering and Moores Cancer Center, University of California San Diego, La Jolla, California 92093, United States

Xinyi Deng,

Corresponding Author Nicole F. Steinmetz – Aiiso Yufeng Li Family Department of Chemical and Nano Engineering, University of California San Diego, La Jolla, California 92093, United States; Shu and K.C. Chien and Peter Farrell Collaboratory, University of California San Diego, San Diego, California 92093, United States; Center for Nano-ImmunoEngineering Moores Cancer Center, Department of Bioengineering, Department of Radiology, Institute for Materials Discovery and Design, and Center for Engineering in Cancer, Institute of Engineering Medicine, University of California San Diego, La Jolla, California 92093, United States; nsteinmetz@ucsd.edu.

[‡]Author Contributions

J.F.A.-d.O. and M.A.M-G. contributed equally. All authors contributed to the writing of this manuscript and approve the final version. N.F.S., J.F.A.O. and M.A.M-G. designed the experiments and analyzed the data. J.S. prepared and purified the PVX particles. Y. M. and X. D. prepared and purified the CPMV particles and carried out the conjugation and characterization of both VNPs. J.F.A.O., Y.M. and X.D. performed all the animal studies. J.F.A.O. and M.A.M-G. performed all in vitro and ex vivo assays. J.F.A.O., M.A.M-G. and N.F.S. wrote the manuscript.

Supporting Information

The Supporting Information is available free of charge at https://pubs.acs.org/doi/10.1021/acs.molpharmaceut.4c00507.

DLS data, antibody titers, additional immunofluorescence imaging data, flow cytometry data, and additional data for TLR7 activation assays (PDF)

The authors declare the following competing financial interest(s): N.F.S. is a co-founder of, has equity in, and has a financial interest in Mosaic ImmunoEnginering Inc.; is a co-founder of and serves as manager of Pokometz Scientific LLC, under which she is a paid consultant to Flagship Labs 95 Inc. and Arana Biosciences Inc.; and is a co-founder and CEO of, has equity in, and has a financial interest in PlantiosX Inc.

Aiiso Yufeng Li Family Department of Chemical and Nano Engineering, University of California San Diego, La Jolla, California 92093, United States; Shu and K.C. Chien and Peter Farrell Collaboratory, University of California San Diego, San Diego, California 92093, United States; Center for Nano-ImmunoEngineering and Moores Cancer Center, University of California San Diego, La Jolla, California 92093, United States

Juliane Schuphan,
Institut für Molekulare Biotechnologie, RWTH Aachen University, 52074 Aachen, Germany

Nicole F. Steinmetz
Aiiso Yufeng Li Family Department of Chemical and Nano Engineering, University of California San Diego, La Jolla, California 92093, United States; Shu and K.C. Chien and Peter Farrell Collaboratory, University of California San Diego, San Diego, California 92093, United States; Center for Nano-ImmunoEngineering Moores Cancer Center, Department of Bioengineering, Department of Radiology, Institute for Materials Discovery and Design, and Center for Engineering in Cancer, Institute of Engineering Medicine, University of California San Diego, La Jolla, California 92093, United States

Abstract

Plant viruses are naturally occurring nanoparticles and adjuvants that interact with the mammalian immune system. This property can be harnessed in vaccines and immunotherapy. We have previously demonstrated that intratumoral immunotherapy with cowpea mosaic virus (CPMV) stimulates systemic and durable antitumor immunity in mouse tumor models and canine cancer patients. Here we compared the antitumor efficacy of CPMV with potato virus X (PVX) using a mouse model B-cell lymphoma (A20 and BALB/c mice). Despite their diverse morphologies and physiochemical properties, both plant viruses elicited systemic and long-lasting antitumor immune memory, preventing the recurrence of A20 lymphoma in rechallenge experiments. Data indicate differences in the underlying mechanism: CPMV persists longer in the tumor microenvironment (TME) compared to PVX; CPMV is a potent and multivalent toll-like receptor (TLR) agonist (activating TLRs 2, 4 and 7) while PVX may only weakly engage with TLR7. While CPMV and PVX recruit myeloid cells (neutrophils)—CPMV also recruits macrophages. Data further indicate that antiviral T cells may play a role in antitumor efficacy in the case of CPMV immunotherapy, however this may not be the case for PVX. Regardless of the mechanism of action, both CPMV and PVX elicited a durable antitumor response against a B-cell lymphoma tumor model and thus are intratumoral immunotherapy candidates for clinical development.

Graphical Abstract

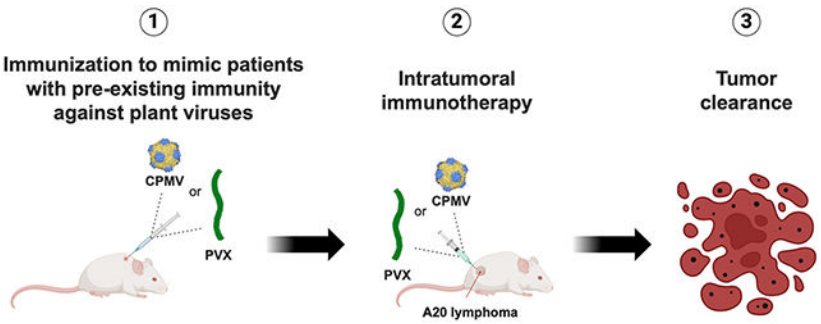

Keywords

plant viruses; cowpea mosaic virus (CPMV); potato virus X (PVX); intratumoral immunotherapy; diffuse large B-cell lymphoma (DLBCL)

INTRODUCTION

Diffuse large B-cell lymphoma (DLBCL) is the most common histological subtype of non-Hodgkin lymphoma and is equally prevalent in both sexes regardless of age.[1-4] The current standard of care is combined chemoimmunotherapy known as R-CHOP (rituximab, cyclophosphamide, doxorubicin, vincristine, and prednisone), achieving a good response and a high survival rate.[2,5] However, depending on the cancer stage at diagnosis, up to 40% of patients experience resistance/relapse due to the heterogeneous and aggressive nature of the disease and drug toxicity.[2] An alternative treatment is passive immunotherapy with monoclonal antibodies,[6,7] but drawbacks include toxicity in nontarget tissues and low efficacy, leading to more frequent recurrence.[4,6,7] This has created a demand for safer and more efficacious therapeutic strategies targeting B-cell neoplasia.

Intratumoral immunotherapy involves the direct administration of immune stimulants into tumors, primarily triggering an innate immune response that increases the infiltration of T cells, and thus overcomes the immunosuppressive tumor microenvironment (TME).[8,9] Effective intratumoral immunotherapy also elicits tumor-specific systemic immunity and long-term antitumor immune memory, preventing recurrence/metastasis.[8,10] B-cell malignancies are predominantly a type of blood cancer, but injectable lesions are often present and are thus suitable for intratumoral immunotherapy, as highlighted by recent clinical trials.[7,11,12]

We have previously shown that plant viruses can be repurposed as a platform technology for intratumoral immunotherapy because they are naturally occurring nanomaterials that interact with innate immune cells, and some plant viruses demonstrate remarkable immunomodulatory properties. Cowpea mosaic virus (CPMV) has shown profound antitumor efficacy when used as intratumoral immunotherapy in mouse tumor models[13-15] and canine cancer patients.[16-19] Plant viruses are inherently safe because they do not infect or replicate in mammalian cells.[20] Instead, they are taken up by innate immune cells and act as agonists for pattern recognition receptors (PRRs),[9] particularly Toll-like receptors (TLRs).

The intratumoral administration of CPMV kick-starts the cancer immunity cell cycle because CPMV is a multivalent TLR agonist (however other features, such as presence of T_{helper} epitopes[21] as well as production of antiviral T cells[22,23] in response to treatment may also play a role in the antitumor mechanism). The repetitive proteinaceous structure of the CPMV capsid activates TLR2 and TLR4 while the single-stranded RNA genome activates TLR7.[9] This remodels the TME and induces an inflammatory response involving type I interferons (IFN), leading to the recruitment, activation, and polarization of innate immune cells (N1 neutrophils, M1 macrophages, dendritic cells) and natural killer cells, which adopt an antitumor phenotype.[9] The interplay between the innate and adaptive immune systems triggered by CPMV intratumoral immunotherapy restores immunosurveillance, leading to systemic and long-lasting antitumor immunity by re-establishing the cancer immunity cell cycle, enhancing tumor antigen presentation, and activating $CD8^+$ effector and memory T cells.[13,18]

Others have shown that papaya mosaic virus (PapMV), a filamentous plant virus,[24] has potency as an intratumoral immunotherapy: the mechanism of action was attributed to the immunomodulatory nature of the packaged ssRNA (here host RNA from the bacterial expression system) activating TLR7 and leading to type I IFNs secretion (especially IFN-α) enhancing $CD8^+$ T cells memory and effector immune response.[25] Using TLR7 knockout (KO) and MyD88 KO mice,[25] immunogenicity and antitumor potency of PapMV was lost.[24] Similar, the dsRNA genome from rice ragged stunt virus is an immunomodulator leading to expression of pro-inflammatory cytokines including type I IFN, resulting in a potent local and systemic antitumor immune response.[26] Other examples, include the use of M13 bacteriophage as cancer immunotherapy; M13 signals through TLR9 based on its packaged ssDNA genome.[27] And last, virus-like particles (VLPs) from Qβ bacteriophage were engineered to package unmethylated CpG oligodeoxynucleotide (CpG ODN) which are TLR9 agonists;[28,29] the latter is being tested in a clinical trial as intratumoral immunotherapy (NCT02680184).

In previous work, we have shown that potato virus X (PVX), another filamentous plant virus, is effective against a mouse model of melanoma, particularly in combination with chemotherapy.[30] Here we revisited PVX and compared its intratumoral immunotherapy efficacy in a BALB/c mouse model of DLBCL (A20). Fluorescence imaging combined with the analysis of TLR signaling provided insights into the changes in the TME following the injection of CMPV and PVX, which are comparable in efficacy but may exert their effects via distinct mechanisms.

MATERIALS AND METHODS

Preparation of Virus Nanoparticles.

CPMV was obtained by the mechanical inoculation of black-eyed pea plants (*Vigna unguiculata* no. 5 from Morgan County Seeds, Lot SW211211075B, Cat# 203) followed by isolation and purification as previously described.[31,32] PVX was isolated from infected *Nicotiana benthamiana* leaves as previously described.[33] Virus nanoparticles (VNPs) labeled with the dye cyanine 5 (Cy5) were prepared by conjugating the sulfoCyanine5 *N*-hydroxysuccinimide (NHS) ester (Lumiprobe) to lysine side chains exposed on the surface

of both viruses as previously described.[34-36] Briefly, a 900-fold molar excess of sulfo-Cy5 NHS was reacted with CPMV or PVX (2 mg/mL in 10 mM potassium phosphate (KP) buffer, pH 7) for 2 h at room temperature. Cy5-CPMV and Cy5-PVX were then purified by ultracentrifugation (1,210,000*g*, 1 h, 4 °C) on a 30% sucrose gradient in 10 mM KP buffer, pH 7. The pellet was resuspended in the same buffer using an orbital shaker overnight at 4 °C. The purified VNPs were stored at 4 °C in the dark.

UV–Vis Spectroscopy.

The concentration of CPMV and PVX was determined using a NanoDrop 2000 spectrophotometer (Thermo Fisher Scientific) and the degree of Cy5 labeling was derived using the Beer–Lambert law ($A_{260} = \varepsilon cl$), where ε is the extinction coefficient, c is the concentration (mg/mL), and l is the path length of the spectrophotometer (0.1 cm). The following extinction coefficients were used for the calculation: CPMV ε_{260nm} = 8.1 mL mg^{-1} cm^{-1}, PVX ε_{260nm} = 2.97 mL mg^{-1} cm^{-1}, and Cy5 ε_{647nm} = 271,000 M^{-1} cm^{-1}.

Agarose Gel Electrophoresis.

CPMV and Cy5-CPMV (10 μg) were mixed with 6× Gel Loading Purple Dye (Biolabs), loaded onto a 1.2% (w/v) agarose gel stained with GelRed (Gold Biotechnologies) in 1× TAE buffer, and electrophoresis was carried out for 30 min at 120 V and 400 mA. The gel was imaged with the ProteinSimple FluorChem R system using the MultiFluor Red channel (607 nm excitation) to visualize Cy5 and UV light to visualize RNA. The gels were then stained with 0.25% (w/v) Coomassie Brilliant Blue G-250 followed by imaging under white light to visualize the protein.

SDS-PAGE.

CPMV and Cy5-CPMV were loaded onto a precast NuPAGE 4–12% Bis–Tris Protein Gel whereas PVX and Cy5-PVX were loaded onto a precast NuPAGE 12% Bis–Tris Protein Gel (both from Invitrogen, Thermo Fisher Scientific). Briefly, 10 μg of each VNP was mixed with 4× lithium dodecylsulfate (LDS) sample buffer (Thermo Fisher Scientific) and NuPAGE sample reducing agent (Invitrogen), followed by denaturation (95 °C for 5 min) prior to loading onto the precast gels. Electrophoresis was carried out at 200 V for 40 min in MOPS buffer (Thermo Fisher Scientific), followed by imaging under the MultiFluor Red channel to detect Cy5 (607 nm excitation). The gels were then stained with GelCode Blue Safe Protein Stain (Thermo Fisher Scientific) followed by imaging under white light to visualize the protein.

Size Exclusion Chromatography.

CPMV and PVX were prepared in 100 mM KP buffer (pH 7) to a final concentration of 0.5 mg/mL. The Cy5-conjugated derivatives were prepared at the same concentration in 10 mM KP buffer, pH 7. All samples were analyzed by size exclusion chromatography (SEC) using the ÄKTA-Pure fast protein liquid chromatography system (GE Healthcare LifeSciences) fitted with a Superose 6 increase 100 GL column operating at a flow rate of 0.5 mL/min. Fractions were eluted using an isocratic profile and absorbance detectors were fixed at 260 nm (nucleic acid), 280 nm (protein), and 647 nm (Cy5).

Transmission Electron Microscopy.

CPMV/Cy5-CPMV (0.1 mg/mL in deionized water) and PVX/Cy5-PVX (0.5 mg/mL in deionized water) were absorbed onto Formvar carbon film-coated transmission electron microscopy (TEM) supports with 400-mesh hexagonal copper grids (Electron Microscopy Sciences). The PELCO easiGlow system was used to increase the hydrophilicity of the grids before loading the VNPs. Following sample incubation, the grids were washed twice with deionized water then stained with 2% (w/v) uranyl acetate (Agar Scientific) and imaged using an FEI Tecnai Spirit G2 BioTWIN transmission electron microscope at 80 kV.

Dynamic Light Scattering.

The hydrodynamic diameter of CPMV (0.2 mg/mL in 100 mM KP buffer, pH7) and Cy5-CPMV (0.2 mg/mL in 10 mM KP buffer, pH7) was measured by dynamic light scattering (DLS) using a Zetasizer Nano ZSP/Zen5600 (Malvern Panalytical). The particle diameter was calculated using the weighted mean of the intensity distributions after three measurements at 25 °C.

Cell Culture and the A20 Lymphoma Tumor Model.

Female BALB/c mice at 7–8 weeks of age (Jackson Laboratory, strain #000651) were used in all experiments, which were carried out as directed by the University of California San Diego's Institutional Animal Care and Use Committee. Mice (n = 10 per group) were preimmunized subcutaneously (s.c.) behind the neck with 100 μg CPMV or PVX in 200 μL sterile PBS (Corning, 21-040-CV) or with sterile PBS as a control. Preimmunization followed a prime-boost biweekly schedule, and blood was collected with lithium-heparin-treated tubes (Thomas Scientific) by retro-orbital bleeding before the first immunization (week 0) and then on weeks 2 and 4. Plasma was collected by centrifugation (2000g, 10 min, 4 °C) and was stored at −20 °C.

A20 murine B-cell lymphoma cells (ATCC) were cultured at 37 °C (5% CO_2) in Roswell Park Memorial Institute 1640 medium (Gibco, Thermo Fisher Scientific), supplemented with 10% (v/v) inactivated-fetal bovine serum (FBS, Gibco), 1% (v/v) Pen/Strep (Thermo Fisher Scientific) and 0.05 mM 2-mercaptoethanol (Gibco). Two weeks after the final immunization, A20 cells were inoculated intradermally (i.d.) into the right flank (200,000 cells in 30 μL sterile PBS) and the mice were monitored every other day for tumor progression. When tumors reached a volume of 30 mm^3 (7–9 days postinoculation), CPMV or PVX was administered intratumorally (i.t.) three times per week at a dose of 100 μg in 20 μL sterile PBS. The control group received sterile PBS. The mice were euthanized if they reached the endpoint tumor volume of ~1500 mm^3. Efficacy studies were repeated at least once to ensure reproducibility. Tumor-free survivors were rechallenged 10 weeks after tumor inoculation (5–6 weeks of tumor remission). A20 cells were intradermally inoculated (i.d.) into the left flank of the survivors (200,000 cells in 30 μL sterile PBS), and the mice were monitored every other day for tumor progression. Age-matched naïve mice (n = 8) were used as controls. Thirty-two days after the tumor rechallenge, the mice were euthanized, and their spleens were harvested for further analysis.

ELISpot Assay.

A murine IFN-γ/IL-4 Double-color enzymatic ELISpot kit assay (Cellular Technology Ltd.) was used to investigate antitumor immune memory. ELISpot plates were coated using a 1:166 dilution of both anti-mouse interleukin-4 (IL-4) capture antibody and anti-mouse interferon-gamma (IFN-γ) capture antibody, overnight at 4 °C, following manufacturer's protocol. The harvested splenocytes from naïve and survivor (rechallenge) mice were plated (500,000 cells/well) followed by stimulation with 100 μL of media alone (negative control), CPMV or PVX (10 μg/mL), A20 cells (500,000 cells/well), or 50 ng/mL phorbol 12-myristate 13-acetate (PMA)/1 mM ionomycin (Sigma-Aldrich, positive control). Plates were incubated at 37 °C and 5% CO_2 for 24 h. Then, plates were washed twice with PBS and twice with PBS plus 0.05% (v/v) Tween-20 (PBST) (200 μL/well) and incubated with anti-mouse IL-4 (biotin-labeled, 1:666 dilution) and antimurine IFN-γ (FITC labeled, 1:1000 dilution) antibodies (80 μL/well), 2 h at room temperature. Plates were washed 3× with PBST (200 μL/well) and incubated with anti-FITC-HRP secondary antibodies (1:1000 dilution) and streptavidin alkaline phosphatase (1:1000 dilution), for 1 h at room temperature (80 μL/well). After another washing step with PBST and 1× distilled water, plates were incubated with alkaline phosphatase substrate for 15 min (room temperature) and washed 3× with distilled water. Then, HRP substrate was added (80 μL/well), followed by an incubation of 10 min (room temperature). Plates were rinsed using tap water (3×) and air-dried overnight (room temperature). Developed spots were quantified using an Immunospot S6 Entry analyzer. Splenocytes were assayed per animal (for CPMV and PVX-treated survivors) and PBS-control splenocytes were pooled. Assays were carried in triplicate for each stimulant.

Antibody Titers.

Anti-CPMV and anti-PVX IgG antibody titers in plasma were detected by enzyme-linked immunosorbent assay (ELISA) in 2-fold serial dilutions of plasma as previously described.[37] The signal was visualized using 1-Step Ultra TMB-ELISA substrate solution (Thermo Fisher Scientific) and quenched with 2 N sulfuric acid (Spectrum Chemical). The absorbance at 450 nm was determined using an Infinite 200 Pro microplate reader and i-control software (Tecan).

Flow Cytometry.

The uptake of Cy5-CPMV and Cy5-PVX by RAW 264.7 macrophages and A20 B-lymphoma cells was tested in the presence and absence of plasma collected from naïve (week 0) or immunized (week 4) mice. A20 B-lymphoma cells (ATCC) were cultivated as described above. RAW 264.7 cells (ATCC) were cultivated at 37 °C (5% CO_2) in Dulbecco's modified Eagle's medium (DMEM) supplemented with 10% (v/v) heat-inactivated FBS and 1% (v/v) Pen/Strep. Cy5-CPMV or Cy5-PVX (1 μg in 50 μL serum-free DMEM per well) were preincubated with plasma (1:200 dilution) or serum-free DMEM in a 96-well v-bottom plate at room temperature for 20 min. RAW 264.7 or A20 cells were then added to the wells (200,000 cells in 50 μL serum-free DMEM per well) and the plate was incubated (37 °C, 5% CO_2) for 2 or 8 h. The plate was then centrifuged (500*g*, 4 min, 4 °C) and washed once with cold sterile PBS and once with cold sterile BD Pharmingen Stain

Buffer (Cat #554656). Cells were then fixed with 4% (v/v) EM-grade paraformaldehyde (15714-S) diluted in 100 μL PBS per well for 10 min on ice, followed by washing once with BD Pharmingen Stain Buffer (100 μL per well) and resuspension in the same buffer (100 μL per well). The cells were kept at 4 °C in the dark before analysis using a BD Acuri C6 Plus flow cytometer with FlowJo v8.6.3 software.

Immunofluorescence Staining.

Mice were preimmunized following the same schedule as described above. A20 cells (200,000 cells in 30 μL sterile PBS) were administered i.d. into the right flank. Mice were monitored every 2 days for signs of tumor progression. Once the tumors reached a volume of 30 mm^3, the animals received a single intratumoral injection of Cy5-CPMV or Cy5-PVX (n = 5, 100 μg in 20 μL PBS) or 20 μL PBS as a control (n = 3). Treated tumors were harvested 24 or 72 h post intratumoral immunotherapy injection and snap frozen in liquid nitrogen. Frozen tumors were embedded in optimal cutting temperature medium (Fisher Healthcare) and 10-μm sections were prepared using a CM1860 cryostat (Leica Microsystems). Tissue sections were then mounted on Superfrost Plus microscope slides (Fisherbrand) for immunofluorescence staining.

The sections were washed in PBS for 5 min before fixing with 4% (v/v) paraformaldehyde in PBS for 10 min at room temperature. The slides were then washed three times with PBS for 5 min, followed by a blocking with 1% (w/v) BSA in PBST for 1 h at room temperature. After another three washes with PBS, the sections were stained with primary antibodies diluted in 1% (w/v) BSA in PBST and incubated overnight at 4 °C in a humidified chamber. The primary antibodies consisted of rabbit anti-mouse CD19 diluted 1:50 (Novus Biologicals, Cat# NBP2-15782), rat anti-mouse Ly-6G/Ly-6C diluted 1:100 (Invitrogen, Cat# 14-5931-82), and rat anti-mouse F4/80 diluted 1:100 (Invitrogen, Cat# MA5-16624). After another three washes, the slides were stained with the secondary antibodies Alexa Fluor 555 goat anti-rabbit IgG (Invitrogen Cat# A-21428) and Alexa Fluor 555 goat anti-rat IgG (Invitrogen Cat# A-21434) diluted 1:1000 in PBST containing 1% (w/v) BSA and incubated for 1 h at room temperature in the dark. After another three washes, the slides were mounted using Fluoroshield with DAPI histology mounting medium (Sigma-Aldrich) for 5–10 min at room temperature and sealed with a 12 mm circular cover glass and nail polish (both from Electron Microscopy Sciences). The slides were stored at 4 °C and were viewed using a Nikon A1R Confocal/TIRF STORM confocal microscope at 20× magnification.

Quantification of the confocal fluorescence images was achieved using the General Analysis module in the Nikon Elements software for image segmentation and quantification of intensity. Each image was analyzed individually, and the total intensity of each color was quantified for statistical analysis using 2-way ANOVA–Tukey's multiple comparisons test using GraphPad Prism v10.2.0 software.

RAW-Blue Cell Activation Assay.

RAW-Blue cells (Invivogen) were seeded at a density of 100,000 cells in 200 μL medium per well in 96-well flat-bottom plates. They were exposed to triplicate samples of CPMV

and PVX (1, 5, 10, and 20 μg per well), a negative control (test medium), or a positive control of 5 μg/mL (defined as 1×) lipopolysaccharide (LPS, Thermo Fisher Scientific). The same VNP concentrations were also tested in the presence and absence of naïve (week 0) or immunized (week 4) mouse plasma. After 24 h incubation (37 °C, 5% CO_2), 20 μL of the supernatant from each well was mixed with 180 μL QUANTI-Blue solution (Invivogen) and incubated (37 °C, 5% CO_2) for 6 h before reading the absorbance at 655 nm using an Infinite 200 Pro microplate reader and i-control software.

TLR7 Agonist Assay.

The TLR7 agonist assay was carried out by Abeomics Inc. using TLR7/NF-κB Luc reporter HEK 293 cells. Briefly, 5×10^4 cells per well were plated in 96-well white solid bottom plates using 100 μL DMEM containing 2 mM L-glutamine, 4.5 g/L glucose, 1 mM sodium pyruvate, 10% (v/v) heat-inactivated FBS and 1% (v/v) Pen/Strep. The cells were incubated for 16 h at 37 °C (5% CO_2) before stimulation with CPMV or PVX (0.03, 0.1, 0.3, 1, 3, 10, 30, or 100 μg/mL) in triplicate for another 16 h at 37 °C (5% CO_2). Resiquimod (R848) was used as a positive control at the same concentration as the VNPs. TLR7 activation was recorded as luciferase activity.

RESULTS AND DISCUSSION

Characterization of CPMV and PVX.

Native CPMV and PVX were propagated in and purified from plants, and the solvent-exposed lysine residues were conjugated to sulfo-Cy5 using NHS chemistry (Figure 1A). Native and denaturing gel electrophoresis confirmed the success of dye conjugation and showed that particle integrity was maintained (Figure 1B,C). Native agarose gel electrophoresis confirmed the colocalization of CPMV RNA, coat protein, and dye in the Cy5-CPMV particles (Figure 1B), but this method was not suitable for the analysis of PVX because the native particles, 515 nm length,[38] are trapped by the pores of the 1.2% (w/v) agarose gel. Denaturing SDS-PAGE confirmed the small coat protein (S-CP, ~24 kDa) and the large coat protein (L-CP, ~42 kDa) of CPMV, and the PVX coat protein with a mass of ~25 kDa (Figure 1C). The colocalization of the fluorescent signal with the coat protein band on the polyacrylamide gels confirmed the successful dye-labeling of CPMV and PVX (Figure 1C). UV–vis spectrophotometry was used to calculate the Cy5 labeling density of both conjugated VNPs, revealing there were ~34 Cy5 dye molecules attached to each CPMV particle and ~191 to each PVX particle (Figure 1D). These differences in labeling density may reflect the different particle sizes/geometries and the number of surface-accessible lysine side chains.[39,40] SEC, TEM and DLS confirmed integrity and homogeneity of the particles. In SEC, the elution profiles of CPMV and PVX from the Superose6 Increase column were coordinated with the Cy5 labels, showing characteristic peaks at ~10–12 and 9 mL, respectively (Figure 1E). The $A_{260/280}$ ratio (1.8 for CPMV and 1.2 for PVX) was not affected by conjugation to Cy5, showing that the particles were not only intact, but also that they did not form aggregates. The colocalization of the elution peak with absorbance at 280 and 647 nm was another indicator of successful Cy5 conjugation. Cy5 absorbance at 647 nm precisely coincided with the ~10–12 and 9 mL elution peaks, confirming the absence of free dye molecules. TEM imaging provided visual confirmation of the intact icosahedral CPMV

and filamentous PVX particles, regardless of dye conjugation (Figure 1F). DLS revealed a hydrodynamic diameter of ~30 nm for CPMV with a narrow polydispersity index of < 0.1 (Figure S1). DLS measures the Stokes radius, which assumes a spherical shape, so this method was not applicable to the analysis of the filamentous PVX particles.[41]

Comparative Antitumor Efficacy of CPMV versus PVX.

Humans are exposed to ubiquitous plant viruses in their food and the environment so it is common to find antibodies against plant viruses in the blood.[37,42,43] But even without pre-existing immunity, antibodies against plant viruses can be elicited following treatment, as we recently showed in canine cancer patients.[17] Our previous research has shown that antibodies against plant viruses tend to enhance the efficacy of intratumoral immunotherapy and hence are not neutralizing.[44] The presence of antiviral antibodies promotes opsonization and uptake by antigen presenting cells (APCs), thus leading to antibody-dependent enhancement of antitumor efficacy.[44] Of note, in clinical trials (NCT02680184) with CpG-loaded Qβ VLPs, patients receiving the intratumoral immunotherapy candidate are first immunized against the VLPs for the same reasons.[28,29] Therefore, we preimmunized female BALB/c mice (n = 10 per group) using a prime-boost regimen (100 μg of CPMV or PVX injected s.c. behind the neck, biweekly during weeks 0 and 2). Blood was collected during weeks 0, 2 and 4, and plasma was screened by ELISA for antibodies against CPMV and PVX (Figure S2). Both treatments elicited potent antibody responses, although the endpoint titer for anti-CPMV antibodies (~1,638,400) was approximately 4-fold higher than that of anti-PVX antibodies (~409,600). This is consistent with previous studies showing that the endocytosis of CPMV by dendritic cells is more efficient, which leads to improved antigen processing and transport to draining lymph nodes (dLNs) compared to PVX.[45] CPMV is also retained in the dLNs for longer, prolonging its interaction with immune cells.[45] Within the dLNs, the antigens are presented to naïve B cells in the germinal centers, initiating a humoral immune response.[46] In contrast, larger particles like PVX drain more slowly and traffic to dLNs less efficiently, reducing their immunogenicity compared to CPMV.[45]

Next tumor treatment studies were performed. Female mice (n = 10 per treatment group) were inoculated i.d. with A20 lymphoma cells 2 weeks after the last immunization and were treated weekly with i.t. injections of CPMV or PXV (100 μg in 20 μL PBS) once the tumors reached ~30 mm^3 in volume. A third group of mice (n = 10) was injected i.t. with PBS as a vehicle control. The tumors were measured every other day. The PBS mice were sacrificed between days 27–36 post-tumor inoculation, when endpoint was reached, but the tumors in the CPMV/PVX treatment groups were less than half this size at the same time point and some animals were tumor-free (Figure 2A). Tumor-free survivors (n = 5 CPMV-treated and n = 3 PVX-treated mice) were monitored for 8 weeks for recurrence following the last intratumoral immunotherapy. These mice were then rechallenged with A20 cells to investigate antitumor immune memory, using a cohort of age-matched mice as a control (Figure 2B,C). No tumorigenesis was observed in the surviving mice from either the CPMV or PVX treatment group, indicating the establishment of immune memory against A20 cells for 30+ days after tumor rechallenge. On day 32 after the tumor rechallenge, spleens were harvested from the survivors and controls and prepared for further analysis.

Isolated splenocytes were stimulated with A20 cells, CPMV, or PVX (with medium as a negative control and PMA/ionomycin as a positive control) and we monitored the responses against A20 cells, CPMV and PVX by counting the number of IFN-γ/IL-4-producing cells using an ELISpot assay (Figures 2D and S3). Both CPMV and PVX intratumoral immunotherapy elicited IFN-γ against A20 cells, consistent with observed antitumor efficacy and immune memory. Differences were noted in the antiviral response, providing the first indication that the two plant viruses work via distinct mechanisms. Specifically, CPMV not only induces a higher antibody titer than PVX, but it also stimulates a strong IFN-γ inflammatory response against the virus itself, whereas the PVX does not (Figure 2D). This likely is attributed to CPMV-specific T cells—previous studies have confirmed that CPMV treatment leads to antiviral T cells,[22,23] and the ELISpot assay is in agreement with this observation. Therefore, T cells directed against CPMV may play a role in the tumor clearance. A20 lymphoma cells can present both endogenous and exogenous antigens due to high expression levels of MHC class I and II molecules[47]—therefore presentation of CPMV exogenous antigens may allow tumor cell elimination through anti-CPMV T cells. Further studies are required to delineate this hypothesis. The same conclusion or hypothesis however cannot be made for PVX: there is no evidence that PVX-specific T cells are elicited (Figure 2D). Lastly, the ELISpot assay showed that the IL-4 response was negligible when compared to the nonstimulated control (Figure S3).

Intratumoral Immunotherapy with CPMV and PVX Recruits Distinct Classes of Innate Immune Cells to Clear B-Cell Lymphoma.

The response of the TME to the intratumoral administration of plant viruses was investigated by preimmunizing female BALB/c mice with a prime-boost regimen consisting of 100 μg CPMV or PVX administered s.c. behind the neck during weeks 0 and 2. A20 tumors were inoculated i.d. 2 weeks after the last immunization, and 100 μg of the Cy5-labeled VNPs was injected once the tumors reached a volume of ~30 mm^3. Tumors were collected 24 or 72 h after treatment for immunofluorescence analysis. PBS was used as a vehicle control for all the treatment steps.

Staining with an anti-mouse CD19 antibody (specific for B cells) revealed a clear difference between tumor regions that were positive and negative for each plant virus (Figure 3A). We observed a sharp decline in the number of B cells in areas containing either CPMV or PVX 24 and 72 h after the intratumoral immunotherapy, indicating tumor cell death (Figure 3B). It is important to note that CPMV or PVX are not directly cytotoxic, the plant viruses recruit innate and adaptive immune cells that induce tumor cell killing. Notably, we detected far fewer PVX than CPMV particles at the 24 h time point, and imaging at 72 h indicated the rapid clearance of PVX, whereas CPMV persisted in the TME (Figure 3C), in line with previous findings.[37] The difference in IFN-γ inflammatory responses between CPMV and PVX may therefore in part reflect the longer residence time of CPMV particles, providing more scope for interactions with immune cells.

CPMV is known to recruit and activate innate immune cells in the TME following intratumoral immunotherapy.[14,22] However, the mechanistic basis of intratumoral immunotherapy with PVX has not been investigated in detail.[30] To date, interactions

between PVX and immune cells have been studied mostly in the context of intraperitoneal, intravenous, and s.c. administration.[45,48] We therefore characterized a subpopulation of innate immune cells within the TME following CPMV-intratumoral immunotherapy or PVX-intratumoral immunotherapy by staining tissue sections with antibodies against the myeloid cell marker Ly-6G/Ly-6C and the macrophage marker F4/80.

Ly-6G is a granulocyte marker[49] expressed on neutrophils, eosinophils, and basophils, which represent 20–30%, 0–7%, and a negligible percentage of mouse granulocytes, respectively.[50] Tumor-infiltrating neutrophils are a key component of cancer immunotherapy because they can promote an antitumor immune response and kill cancer cells.[51,52] Ly-6C is expressed on monocytes, which can differentiate into macrophages, M-MDSCs or dendritic cells after tumor infiltration.[53] M1 macrophages and dendritic cells within the tumor are antitumor cells because they present antigens and promote inflammation.[53] Hence Ly-6G/Ly-6C is a myeloid marker for neutrophils and monocytes. F4/80 has been extensively utilized as a murine macrophage marker since it is highly expressed by a wide variety of tissue macrophages.[54]

We observed the colocalization of both CPMV and PVX with tumor-infiltrating myeloid cells 24 h postintratumoral immunotherapy, despite the rapid clearance of PVX (Figures 4A and 3C). Remarkably, even though the PVX signal was much weaker than the CPMV signal after 72 h, the number of myeloid cells in the tumor was similar (Figures 4A,C and S4). We hypothesize that PVX compensates for its rapid clearance by leaving behind a strong immune cell population.

Tumor-associated macrophages are the most prevalent innate immune cells within the TME,[55] and depending on their phenotype they can delay tumor progression by bridging the innate and adaptive immune systems, making an important contribution to the efficacy of immunotherapy.[22,56] CPMV was colocalized with macrophages 24 and 72 h postintratumoral immunotherapy (Figure 4B,D). However, our data clearly show that PVX does not recruit or interact with the macrophage population in the TME at either time point (Figures 4B and S5). These results suggest that the antitumor immunity elicited by CPMV is mediated by interactions with neutrophils/monocytes and macrophages whereas PVX appears to act via neutrophils/monocytes alone, however future studies are needed to dissect which subtypes of cells respond to CPMV vs PVX intratumoral immunotherapy. It is still unclear whether the cells recruited by CPMV or PVX are tumor cell killing cells or they mediate recruitment and activation of other subsets of cells leading to the observed potent and durable efficacy.

Cellular Uptake and Immunogenicity of CPMV and PVX.

We compared the uptake of CPMV and PVX particles into macrophages by incubating RAW 264.7 cells (a mouse macrophage cell line) with the Cy5-CPMV or Cy5-PVX particles in the presence and absence of plasma from immunized mice, with plasma from naïve mice as control. Even though PVX did not interact with or recruit macrophages in the tumor model, this is still a suitable model to investigate nanoparticle–cell interactions in vitro. Cy5-CPMV or Cy5-PVX particles were incubated with plasma from immunized mice (1:200, to simulate opsonization) or from naïve mice for 20 min before adding Cy5-CPMV or

Cy5-PVX particles to the RAW 264.7 cells in serum-free medium (to minimize nonspecific interactions with other media components) and incubating for 2 or 8 h at 37 °C. After several washing steps to remove excess Cy5-CPMV or Cy5-PVX particles, we measured the mean fluorescence intensity of the cells to quantify the efficiency of uptake (Figure 5A). The uptake of either CPMV or PVX was observed and increased over time; as expected, the presence of anti-CPMV/PVX antibodies dramatically enhanced uptake.[44] CPMV was taken up 8-fold more efficiently when preincubated with plasma from immunized rather than naïve mice. The same opsonization effect was observed for PVX, but the enhancement was only 1.5-fold in this case. The uptake of opsonized CPMV particles was twice as efficient as the opsonized PVX particles after 2 h, and eight times as efficient after 8 h (Figures 5A and S6).

Macrophages, monocytes, and dendritic cells take up particles, cell debris, and dead cells primarily by phagocytosis, which can take from 30 min to several hours depending on the cell type and the size, shape, and surface composition of the particles.[57] The plant viruses are likely to undergo opsonization in vivo by specific antibodies elicited by the multiple doses, and the Fc region of such antibodies binds to receptors on the surface of APCs, thus increasing the efficiency of internalization.[57] Elongated particles may evade phagocyte uptake, prolonging their circulation in vivo, whereas spherical nanoparticles are taken up rapidly, potentially explaining the differential uptake of CPMV and PVX by RAW 264.7 cells.[45,58]

Finally, we used RAW-Blue cells (derived from RAW 264.7 cells) expressing a variety of PRRs (including TLRs, NOD1 and NOD2 receptors, RIG-1, and C-type lectin receptors) to investigate the immunogenicity of CPMV or PVX in a QUANTI-Blue assay.[40,59] When RAW-Blue cells are stimulated, the transcription factors AP-1 and NF-κB activate a reporter gene encoding secreted embryonic alkaline phosphatase (SEAP), which is then detected in the medium to quantify the response. We tested different concentrations of CPMV or PVX (1, 5, 10, and 20 μg per 100,000 cells for 24 h), using bacterial LPS as a positive control and nonstimulated cells as a negative control. We also determined the effect of incubating CPMV or PVX with plasma from naïve or immunized mice before exposing the cells.

RAW-Blue cells were activated in a concentration-dependent manner by CPMV (there was an approximate 2-fold difference between concentrations), and activation was slightly more efficient when the CPMV was opsonized in the presence of anti-CPMV antibodies (Figure 5B). This is consistent with our prior work demonstrating that CPMV is a TLR-2, 4, 7 agonist.[9] In stark contrast, the levels of SEAP detected following treatment with PVX were similar to the negative control—only in the presence of anti-PVX sera, negligible yet statistically significant PRR activation was indicated (Figure 5B).

To gain more insights into whether PVX activates TLR7 (based on its ssRNA genome), we investigated the activation of TLR7 signaling directly using a TLR7/NF-κB Luc reporter cell line (Figure S7). Due to assay limitations, the moderate TLR7 signaling from CPMV stimulation lead to an incomplete EC50 curve—therefore the EC_{50} value should be regarded as estimation at best—we determined an EC_{50} of 689 μg/mL for CPMV compared to the positive control R848 with an EC_{50} of 1.15 μg/mL (Figure 5C). Consistent with the RAW-Blue assay, there is no evidence that PVX is a TLR7 agonist in the absence of

anti-PVX antibodies (EC_{50} > 1000 μg/mL, Figure 5C). The relatively weak TLR7 priming by CPMV and lack thereof of PVX may indicate that either the in vitro assays are not suitable for studying TLR7 activation by plant viruses. Previous assays by others delineated that the ssRNA genome of PVX acts indeed acts as an adjuvant and signals via TLR7; vaccine studies showed reduced efficacy in TLR7 KO mice indicating TLR7 plays a role in its function as adjuvant.[60]

Whether TLR7 signaling is a key component to determine effectiveness of plant virus-based adjuvants and their use as intratumoral immunotherapy agents remains elusive. In fact, we have previously shown that empty CPMV (lacking genomic RNA) and native, RNA-containing CPMV have antitumor efficacy, eliciting a systemic immune response in mouse tumor models[13,15,61] and canine cancer patients.[16,17,19] While native, RNA-containing CPMV was found to be more potent, also the RNA-free counterpart demonstrated highly potent efficacy.[16] It is clear that plant viruses engage with immune cells through multiple axes and more research is needed to delineate the distinct mechanisms by which plant virus platform technologies activate antitumor immunity.

CONCLUSION

We have shown that two morphologically distinct plant viruses can elicit durable and systemic antitumor immune responses against an aggressive B-cell lymphoma tumor model. We[14,62] and others[24,63,64] have developed cancer immunotherapy candidates based on other plant viruses due to their ability to reprogram the TME. The intratumoral administration of plant viruses results in their interaction with and activation of innate immune cells within the TME—for some plant viruses—via the recognition of PRR such as TLRs, restarting the cancer immunity cycle.[48] Here we compared the antitumor efficacy of CPMV vs PVX. Although PVX has a filamentous structure and CPMV is icosahedral, they elicited antitumor immune responses of similar potency. Our data indicate that CPMV and PVX have differential tumor residence time with PVX being cleared more rapidly. Both CPMV and PVX recruit high amounts of myeloid cells, but only CPMV recruits macrophages. This data highlights that various classes of plant viruses may serve as potent tools for cancer immunotherapy; our data also indicates that different plant virus platform technologies prime antitumor immunity through distinct immunomodulatory pathways. More research is required to determine the precise mechanism underlying the antitumor immune responses elicited by the different classes of plant viruses. However, it is clear, that diverse plant viruses are suitable as safe and efficacious cancer immunotherapy candidates that elicit long-lasting and systemic antitumor immune responses and could prevent metastasis and recurrence in human patients.

Supplementary Material

Refer to Web version on PubMed Central for supplementary material.

ACKNOWLEDGMENTS

The authors thank the University of California, San Diego Cellular and Molecular Medicine Electron Microscopy Core (UCSD-CMM-EM Core, RRID: SCR_022039) for equipment access and technical assistance. The UCSD-

CMM-EM Core is partly supported by NIH award number S10OD023527. The authors thank the Kersi Pestonjamasp and UCSD Cancer Center Microscopy Shared Facility (Specialized Support Grant P30 CA23100-28 and 2P30CA023100 by NCI) for providing equipment, services, and expertise to complete this work.

Funding

This work was supported in part by NIH (R01-CA224605, R01 CA274640 and R01-CA253615, R01-CA253615-02S1 to N.F.S.), UC San Diego Materials Research Science and Engineering Center (UCSD MRSEC), supported by the National Science Foundation (Grant DMR-2011924), San Diego, and the American Cancer Society and F.M. Kirby Foundation Inc. Mission Boost Grant, MBGI-23-1030244-01-MBG.

REFERENCES

(1). Mamgain G; Singh PK; Patra P; Naithani M; Nath UK Diffuse large B-cell lymphoma and new insights into its pathobiology and implication in treatment. J. Family Med. Prim. Care 2022, 11 (8), 4151–4158. [PubMed: 36353039]

(2). Bakhshi TJ; Georgel PT Genetic and epigenetic determinants of diffuse large B-cell lymphoma. Blood Cancer J. 2020, 10 (12), 123. [PubMed: 33277464]

(3). Guja K; Liehr T; Rincic M; Kosyakova N; Hussein Azawi SS Molecular Cytogenetic Characterization Identified the Murine B-Cell Lymphoma Cell Line A-20 as a Model for Sporadic Burkitt's Lymphoma. J. Histochem. Cytochem 2017, 65 (11), 669–677. [PubMed: 28902524]

(4). Palmieri C; Falcone C; Iaccino E; Tuccillo FM; Gaspari M; Trimboli F; De Laurentiis A; Luberto L; Pontoriero M; Pisano A; et al. In vivo targeting and growth inhibition of the A20 murine B-cell lymphoma by an idiotype-specific peptide binder. Blood 2010,116 (2), 226–238. [PubMed: 20363775]

(5). Coiffier B; Sarkozy C Diffuse large B-cell lymphoma: R-CHOP failure-what to do? Hematology Am. Soc. Hematol Educ. Program 2016, 2016 (1), 366–378. [PubMed: 27913503]

(6). Modi D; Potugari B; Uberti J Immunotherapy for Diffuse Large B-Cell Lymphoma: Current Landscape and Future Directions. Cancers 2021, 13 (22), 5827. [PubMed: 34830980]

(7). Brody JD; Ai WZ; Czerwinski DK; Torchia JA; Levy M; Advani RH; Kim YH; Hoppe RT; Knox SJ; Shin LK; et al. In situ vaccination with a TLR9 agonist induces systemic lymphoma regression: a phase I/II study. J. Clin. Oncol 2010, 28 (28), 4324–4332. [PubMed: 20697067]

(8). Hong WX; Haebe S; Lee AS; Westphalen CB; Norton JA; Jiang W; Levy R Intratumoral Immunotherapy for Early-stage Solid Tumors. Clin. Cancer Res 2020, 26 (13), 3091–3099. [PubMed: 32071116]

(9). Mao C; Beiss V; Fields J; Steinmetz NF; Fiering S Cowpea mosaic virus stimulates antitumor immunity through recognition by multiple MYD88-dependent toll-like receptors. Biomaterials 2021, 275, 120914. [PubMed: 34126409]

(10). Gorbet MJ; Singh A; Mao C; Fiering S; Ranjan A Using nanoparticles for in situ vaccination against cancer: mechanisms and immunotherapy benefits. Int. J. Hyperthermia 2020, 37 (3), 18–33. [PubMed: 33426995]

(11). Melero I; Castanon E; Alvarez M; Champiat S; Marabelle A Intratumoural administration and tumour tissue targeting of cancer immunotherapies. Nat. Rev. Clin. Oncol 2021, 18 (9), 558–576. [PubMed: 34006998]

(12). Shree T; Haebe S; Czerwinski DK; Eckhert E; Day G; Sathe A; Grimes S; Frank MJ; Maeda LS; Alizadeh AA; et al. A clinical trial of therapeutic vaccination in lymphoma with serial tumor sampling and single-cell analysis. Blood Adv. 2024, 8 (1), 130–142. [PubMed: 37939259]

(13). Lizotte PH; Wen AM; Sheen MR; Fields J; Rojanasopondist P; Steinmetz NF; Fiering S In situ vaccination with cowpea mosaic virus nanoparticles suppresses metastatic cancer. Nat. Nanotechnol 2016, 11 (3), 295–303. [PubMed: 26689376]

(14). Shukla S; Wang C; Beiss V; Cai H; Washington T; Murray AA; Gong X; Zhao Z; Masarapu H; Zlotnick A; et al. The unique potency of Cowpea mosaic virus (CPMV) in situ cancer vaccine. Biomater. Sci 2020, 8 (19), 5489–5503. [PubMed: 32914796]

(15). Wang C; Beiss V; Steinmetz NF Cowpea Mosaic Virus Nanoparticles and Empty Virus-Like Particles Show Distinct but Overlapping Immunostimulatory Properties. J. Virol 2019, 93(21), No. e00129–19. [PubMed: 31375592]

(16). Alonso-Miguel D; Valdivia G; Guerrera D; Perez-Alenza MD; Pantelyushin S; Alonso-Diez A; Beiss V; Fiering S; Steinmetz NF; Suarez-Redondo M; et al. Neoadjuvant in situ vaccination with cowpea mosaic virus as a novel therapy against canine inflammatory mammary cancer. J. Immunother. Cancer 2022, 10 (3), No. e004044. [PubMed: 35277459]

(17). Valdivia G; Alonso-Miguel D; Perez-Alenza MD; Zimmermann ABE; Schaafsma E; Kolling F. W. t. ; Barreno L; Alonso-Diez A; Beiss V; Affonso de Oliveira JF; et al. Neoadjuvant Intratumoral Immunotherapy with Cowpea Mosaic Virus Induces Local and Systemic Antitumor Efficacy in Canine Mammary Cancer Patients. Cells 2023, 12 (18), 2241. [PubMed: 37759464]

(18). Barreno L; Sevane N; Valdivia G; Alonso-Miguel D; Suarez-Redondo M; Alonso-Diez A; Fiering S; Beiss V; Steinmetz NF; Perez-Alenza MD; et al. Transcriptomics of Canine Inflammatory Mammary Cancer Treated with Empty Cowpea Mosaic Virus Implicates Neutrophils in Anti-Tumor Immunity. Int. J. Mol. Sci 2023, 24 (18), 14034. [PubMed: 37762335]

(19). Hoopes PJ; Wagner RJ; Duval K; Kang K; Gladstone DJ; Moodie KL; Crary-Burney M; Ariaspulido H; Veliz FA; Steinmetz NF; et al. Treatment of Canine Oral Melanoma with Nanotechnology-Based Immunotherapy and Radiation. Mol. Pharmaceutics 2018, 15 (9), 3717–3722.

(20). Omole AO; Affonso de Oliveira J; Sutorus L; Karan S; Zhao Z; Neun BW; Cedrone E; Clogston JD; Xu J; Sierk M; Chen Q; Meerzaman D; Dobrovolskaia MA; Steinmetz NF Cellular fate of a plant virus immunotherapy candidate. Commun Biol 2024, 7, 1382. [PubMed: 39443610]

(21). Bachmann MF; Jennings GT Vaccine delivery: a matter of size, geometry, kinetics and molecular patterns. Nat. Rev. Immunol 2010, 10 (11), 787–796. [PubMed: 20948547]

(22). Wang C; Fiering SN; Steinmetz NF Cowpea Mosaic Virus Promotes Anti-Tumor Activity and Immune Memory in a Mouse Ovarian Tumor Model. Adv. Ther 2019, 2 (5), 1900003.

(23). Mao C; Beiss V; Ho GW; Fields J; Steinmetz NF; Fiering S In situ vaccination with cowpea mosaic virus elicits systemic antitumor immunity and potentiates immune checkpoint blockade. J. Immunother. Cancer 2022, 10 (12), No. e005834. [PubMed: 36460333]

(24). Lebel ME; Chartrand K; Tarrab E; Savard P; Leclerc D; Lamarre A Potentiating Cancer Immunotherapy Using Papaya Mosaic Virus-Derived Nanoparticles. Nano Lett. 2016, 16 (3), 1826–1832. [PubMed: 26891174]

(25). Lebel ME; Daudelin JF; Chartrand K; Tarrab E; Kalinke U; Savard P; Labrecque N; Leclerc D; Lamarre A Nanoparticle adjuvant sensing by TLR7 enhances CD8+ T cell-mediated protection from Listeria monocytogenes infection. J. Immunol 2014, 192 (3), 1071–1078. [PubMed: 24376264]

(26). Mohammadi N; Nouri F; Asgari Y; Moradi-Sardareh H; Sharafi-Kolkeshvandi M; Nemati H; Kardar GA The immunostimulant effects of the rice ragged stunt virus genome on the growth and metastasis of breast cancer in mouse model. Int. Immunopharmacol 2023, 125 (Pt A), 111101. [PubMed: 37922568]

(27). Wang HY; Chang YC; Hu CW; Kao CY; Yu YA; Lim SK; Mou KY Development of a Novel Cytokine Vehicle Using Filamentous Phage Display for Colorectal Cancer Treatment. ACS Synth. Biol 2021, 10 (8), 2087–2095. [PubMed: 34342970]

(28). Sabree SA; Voigt AP; Blackwell SE; Vishwakarma A; Chimenti MS; Salem AK; Weiner GJ Direct and indirect immune effects of CMP-001, a virus-like particle containing a TLR9 agonist. J. Immunother. Cancer 2021, 9 (6), No. e002484. [PubMed: 34083419]

(29). Lemke-Miltner CD; Blackwell SE; Yin C; Krug AE; Morris AJ; Krieg AM; Weiner GJ Antibody Opsonization of a TLR9 Agonist-Containing Virus-like Particle Enhances In Situ Immunization. J. Immunol 2020, 204 (5), 1386–1394. [PubMed: 31953355]

(30). Lee KL; Murray AA; Le DHT; Sheen MR; Shukla S; Commandeur U; Fiering S; Steinmetz NF Combination of Plant Virus Nanoparticle-Based in Situ Vaccination with Chemotherapy Potentiates Antitumor Response. Nano Lett. 2017, 17 (7), 4019–4028. [PubMed: 28650644]

(31). Wen AM; Lee KL; Yildiz I; Bruckman MA; Shukla S; Steinmetz NF Viral nanoparticles for in vivo tumor imaging. J. Vis. Exp 2012, No. 69, No. e4352. [PubMed: 23183850]

(32). Wellink J. Comovirus isolation and RNA extraction. Methods Mol. Biol 1998, 81, 205–209. [PubMed: 9760508]

(33). Lee KL; Uhde-Holzem K; Fischer R; Commandeur U; Steinmetz NF Genetic engineering and chemical conjugation of potato virus X. Methods Mol. Biol 2014, 1108, 3–21. [PubMed: 24243237]

(34). Le DHT; Hu H; Commandeur U; Steinmetz NF Chemical addressability of potato virus X for its applications in bio/nanotechnology. J. Struct. Biol 2017, 200 (3), 360–368. [PubMed: 28647539]

(35). Wang Q; Kaltgrad E; Lin T; Johnson JE; Finn MG Natural Supramolecular Building Blocks. Chem. Biol 2002, 9 (7), 805–811. [PubMed: 12144924]

(36). Wen AM; Infusino M; De Luca A; Kernan DL; Czapar AE; Strangi G; Steinmetz NF Interface of physics and biology: engineering virus-based nanoparticles for biophotonics. Bioconjug. Chem 2015, 26 (1), 51–62. [PubMed: 25541212]

(37). Affonso de Oliveira JF; Chan SK; Omole AO; Agrawal V; Steinmetz NF In Vivo Fate of Cowpea Mosaic Virus In Situ Vaccine: Biodistribution and Clearance. ACS Nano 2022, 16 (11), 18315–18328. [PubMed: 36264973]

(38). Serwer P. Agarose gel electrophoresis of bacteriophages and related particles. J. Chromatogr 1987, 418, 345–357. [PubMed: 3305547]

(39). Steinmetz NF; Mertens ME; Taurog RE; Johnson JE; Commandeur U; Fischer R; Manchester M Potato virus X as a novel platform for potential biomedical applications. Nano Lett. 2010, 10 (1), 305–312. [PubMed: 20017489]

(40). Chariou PL; Beiss V; Ma Y; Steinmetz NF In situ vaccine application of inactivated CPMV nanoparticles for cancer immunotherapy. Mater. Adv 2021, 2 (5), 1644–1656. [PubMed: 34368764]

(41). Simone EA; Dziubla TD; Colon-Gonzalez F; Discher DE; Muzykantov VR Effect of polymer amphiphilicity on loading of a therapeutic enzyme into protective filamentous and spherical polymer nanocarriers. Biomacromolecules 2007, 8 (12), 3914–3921. [PubMed: 18038999]

(42). Aguado-Garcia Y; Taboada B; Moran P; Rivera-Gutierrez X; Serrano-Vazquez A; Isa P; Rojas-Velazquez L; Perez-Juarez H; Lopez S; Torres J; et al. Tobamoviruses can be frequently present in the oropharynx and gut of infants during their first year of life. Sci. Rep 2020, 10 (1), 13595. [PubMed: 32788688]

(43). Liu R; Vaishnav RA; Roberts AM; Friedland RP Humans have antibodies against a plant virus: evidence from tobacco mosaic virus. PLoS One 2013, 8 (4), No. e60621. [PubMed: 23573274]

(44). Shukla S; Wang C; Beiss V; Steinmetz NF Antibody Response against Cowpea Mosaic Viral Nanoparticles Improves In Situ Vaccine Efficacy in Ovarian Cancer. ACS Nano 2020, 14 (3), 2994–3003. [PubMed: 32133838]

(45). Shukla S; Myers JT; Woods SE; Gong X; Czapar AE; Commandeur U; Huang AY; Levine AD; Steinmetz NF Plant viral nanoparticles-based HER2 vaccine: Immune response influenced by differential transport, localization and cellular interactions of particulate carriers. Biomaterials 2017, 121, 15–27. [PubMed: 28063980]

(46). Wagar LE; Salahudeen A; Constantz CM; Wendel BS; Lyons MM; Mallajosyula V;Jatt LP; Adamska JZ; Blum LK; Gupta N; et al. Modeling human adaptive immune responses with tonsil organoids. Nat. Med 2021, 27 (1), 125–135. [PubMed: 33432170]

(47). Staveley-O'Carroll K; Sotomayor E; Montgomery J; Borrello I; Hwang L; Fein S; Pardoll D; Levitsky H Induction of antigen-specific T cell anergy: An early event in the course of tumor progression. Proc. Natl. Acad. Sci. U.S.A 1998, 95 (3), 1178–1183. [PubMed: 9448305]

(48). Shukla S; Roe AJ; Liu R; Veliz FA; Commandeur U; Wald DN; Steinmetz NF Affinity of plant viral nanoparticle potato virus X (PVX) towards malignant B cells enables cancer drug delivery. Biomater. Sci 2020, 8 (14), 3935–3943. [PubMed: 32662788]

(49). Daley JM; Thomay AA; Connolly MD; Reichner JS; Albina JE Use of Ly6G-specific monoclonal antibody to deplete neutrophils in mice. J. Leukoc. Biol 2008, 83 (1), 64–70. [PubMed: 17884993]

(50). O'Connell KE; Mikkola AM; Stepanek AM; Vernet A; Hall CD; Sun CC; Yildirim E; Staropoli JF; Lee JT; Brown DE Practical murine hematopathology: a comparative review and implications for research. Comp. Med 2015, 65 (2), 96–113. [PubMed: 25926395]

(51). Furumaya C; Martinez-Sanz P; Bouti P; Kuijpers TW; Matlung HL Plasticity in Pro- and Anti-tumor Activity of Neutrophils: Shifting the Balance. Front. Immunol 2020, 11, 2100. [PubMed: 32983165]

(52). Wang X; Qiu L; Li Z; Wang XY; Yi H Understanding the Multifaceted Role of Neutrophils in Cancer and Autoimmune Diseases. Front. Immunol 2018, 9, 2456. [PubMed: 30473691]

(53). Chen X; Li Y; Xia H; Chen YH Monocytes in Tumorigenesis and Tumor Immunotherapy. Cells 2023, 12 (13), 1673. [PubMed: 37443711]

(54). Dos Anjos Cassado A. F4/80 as a Major Macrophage Marker: The Case of the Peritoneum and Spleen. Results Probl. Cell Differ 2017, 62, 161–179. [PubMed: 28455709]

(55). He Z; Zhang S Tumor-Associated Macrophages and Their Functional Transformation in the Hypoxic Tumor Microenvironment. Front. Immunol 2021, 12, 741305. [PubMed: 34603327]

(56). Pan Y; Yu Y; Wang X; Zhang T Tumor-Associated Macrophages in Tumor Immunity. Front. Immunol 2020, 11, 583084. [PubMed: 33365025]

(57). Behzadi S; Serpooshan V; Tao W; Hamaly MA; Alkawareek MY; Dreaden EC; Brown D; Alkilany AM; Farokhzad OC; Mahmoudi M Cellular uptake of nanoparticles: journey inside the cell. Chem. Soc. Rev 2017, 46 (14), 4218–4244. [PubMed: 28585944]

(58). Shukla S; Wen AM; Ayat NR; Commandeur U; Gopalkrishnan R; Broome AM; Lozada KW; Keri RA; Steinmetz NF Biodistribution and clearance of a filamentous plant virus in healthy and tumor-bearing mice. Nanomedicine 2014, 9 (2), 221–235. [PubMed: 23834501]

(59). Jung E; Chung YH; Steinmetz NF TLR Agonists Delivered by Plant Virus and Bacteriophage Nanoparticles for Cancer Immunotherapy. Bioconjug. Chem 2023, 34 (9), 1596–1605. [PubMed: 37611278]

(60). Jobsri J; Allen A; Rajagopal D; Shipton M; Kanyuka K; Lomonossoff GP; Ottensmeier C; Diebold SS; Stevenson FK; Savelyeva N Plant virus particles carrying tumour antigen activate TLR7 and Induce high levels of protective antibody. PLoS One 2015, 10 (2), No. e0118096. [PubMed: 25692288]

(61). Kerstetter-Fogle A; Shukla S; Wang C; Beiss V; Harris PLR; Sloan AE; Steinmetz NF Plant Virus-Like Particle In Situ Vaccine for Intracranial Glioma Immunotherapy. Cancers 2019, 11 (4), 515. [PubMed: 30974896]

(62). Beiss V; Mao C; Fiering SN; Steinmetz NF Cowpea Mosaic Virus Outperforms Other Members of the Secoviridae as In Situ Vaccine for Cancer Immunotherapy. Mol. Pharmaceutics 2022, 19 (5), 1573–1585.

(63). Chartrand K; Lebel ME; Tarrab E; Savard P; Leclerc D; Lamarre A Efficacy of a Virus-Like Nanoparticle As Treatment for a Chronic Viral Infection Is Hindered by IRAK1 Regulation and Antibody Interference. Front. Immunol 2018, 8, 1885. [PubMed: 29354118]

(64). Shahgolzari M; Venkataraman S; Osano A; Akpa PA; Hefferon K Plant Virus Nanoparticles Combat Cancer. Vaccines 2023, 11 (8), 1278. [PubMed: 37631846]

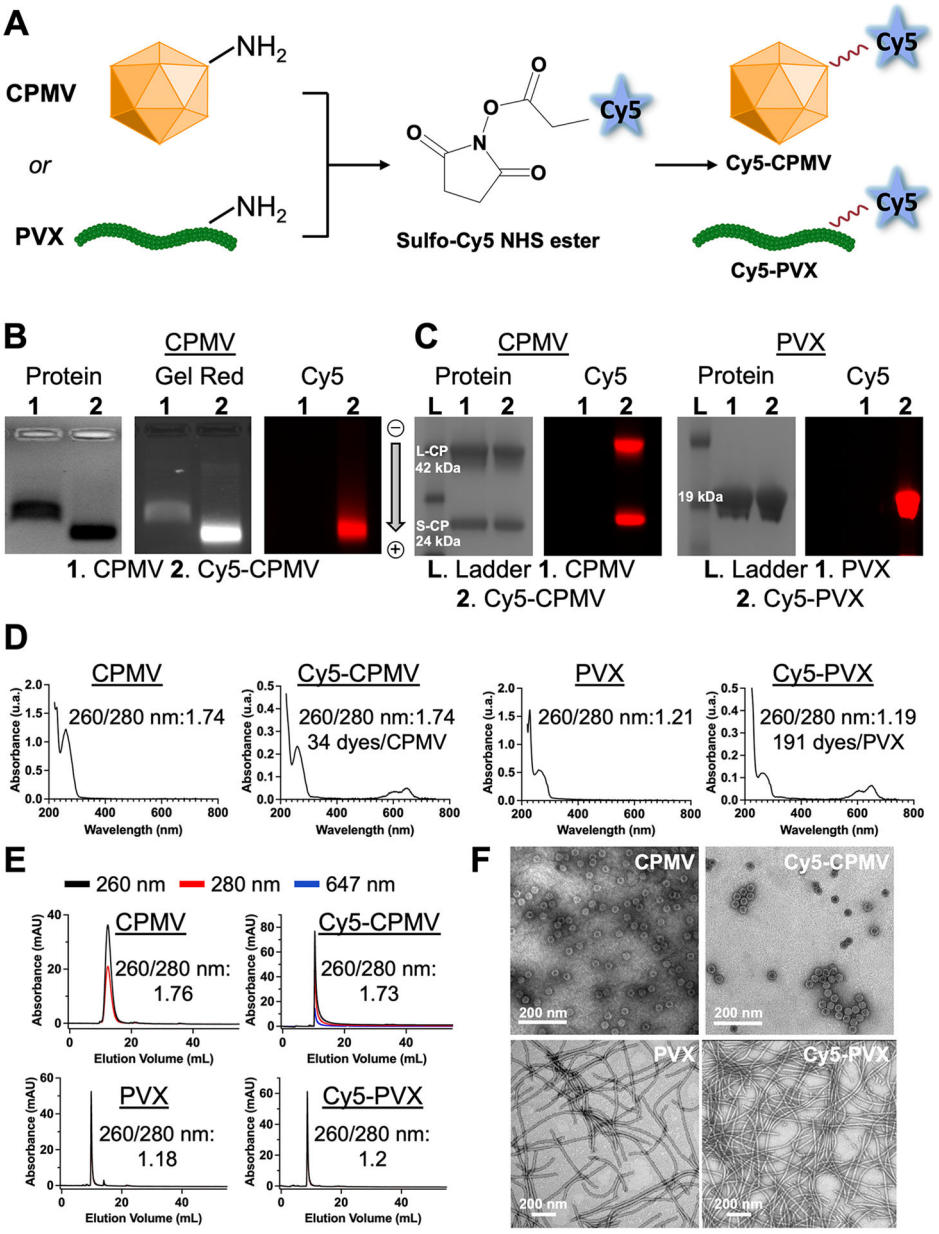

Figure 1.

Intact CPMV and PVX were purified and conjugated with Cy5 fluorophores. (A) Schematic showing the conjugation of sulfo-Cy5 to surface-exposed lysine residues on CPMV and PVX using NHS chemistry. Virus structures were sourced from Biorender.com and the reaction scheme was created using ChemDraw Ultra 7.0. (B) CPMV native agarose gel stained with GelRed (to visualize nucleic acid, imaged under UV light) and Coomassie Brilliant Blue (to visualize protein, imaged under white light). (C) CPMV small (S-CP, 24 kDa) and large (L-CP; 42 kDa) coat proteins were separated on a denaturing 4–12% Nu-PAGE gel and the PVX coat protein (19 kDa) was separated on a denaturing 12% Nu-PAGE gel. The gels were incubated with GelCode Blue Safe protein stain and imaged under white light. Before protein staining, Cy5 was imaged in the native and denaturing gels

using the MultiFluor Red channel (607 nm excitation) on a FluorChem R imager. (D) UV–vis spectra of all purified and Cy5-conjugated VNPs, also showing the $A_{260/280}$ ratio and labeling density. (E) SEC profiles. Cy5 was detected and the $A_{260/280}$ ratio is also shown. (F) TEM images of negatively stained purified and conjugated VNPs. The image data were analyzed using ImageJ.

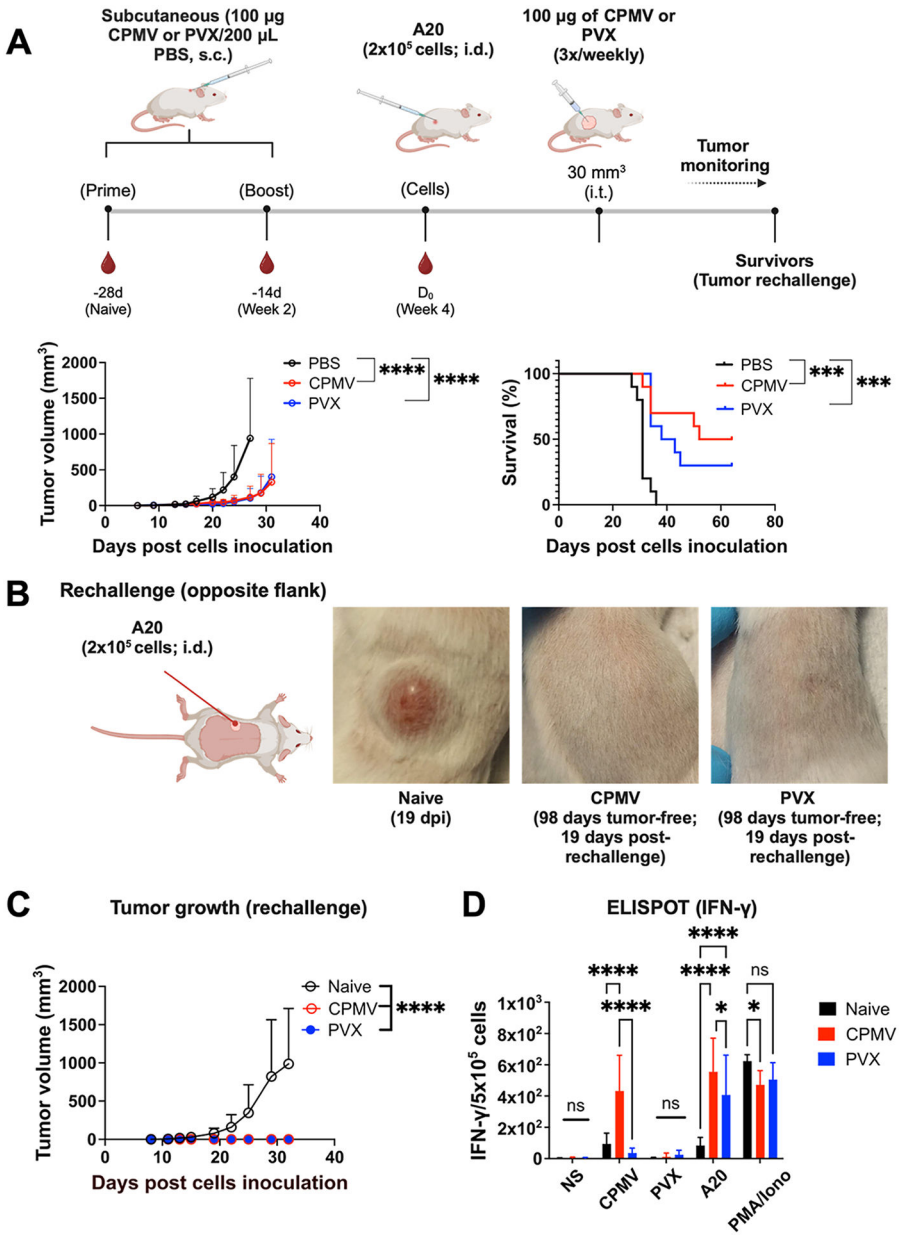

Figure 2.

CPMV and PVX induce antitumor efficacy and immune memory against the A20 tumor model. (A) Female BALB/c mice (n = 10 per group) were immunized in a prime-boost schedule (100 μg VNP in 200 μL of PBS) s.c. behind the neck. Blood was collected 2 weeks after each injection. A20 lymphoma cells (2×10^5 cells/mouse) were inoculated i.d. into the right flank. When the tumors reached ~30 mm^3 in volume, CPMV or PVX (100 μg/20 μL of PBS) or PBS (control) was injected intratumorally (i.t.) three times per week and the tumor volume was monitored every other day. Survival curves are shown for all treatment groups. Data are means ± SD for at least n = 5 per group. (B,C) Survivors (CPMV n = 5 and PVX n = 3) were rechallenged (A20 lymphoma cells, 2×10^5 cells/mouse, i.d., opposite flank) and an age-matched (n = 8) set of mice was used

as a tumor growth control. No treatment was administered (only tumor monitoring). (D) After 32 days, the mice were euthanized, spleens were harvested, and splenocytes (5×10^5 cells/well) were stimulated with medium only (NS), CPMV, PVX, A20 cells (5×10^5 cells/well) or PMA/ionomycin (positive control). IFN γ-producing cells were counted among the splenocyte-forming colonies. Statistical significance was determined by two-way ANOVA using pairwise multiple comparison followed by Tukey's multiple comparisons test to compare groups (****$p < 0.0001$). Survival curves were compared using the log-rank (Mantel–Cox) test (***$p < 0.001$) in GraphPad Prism v10.2.0.

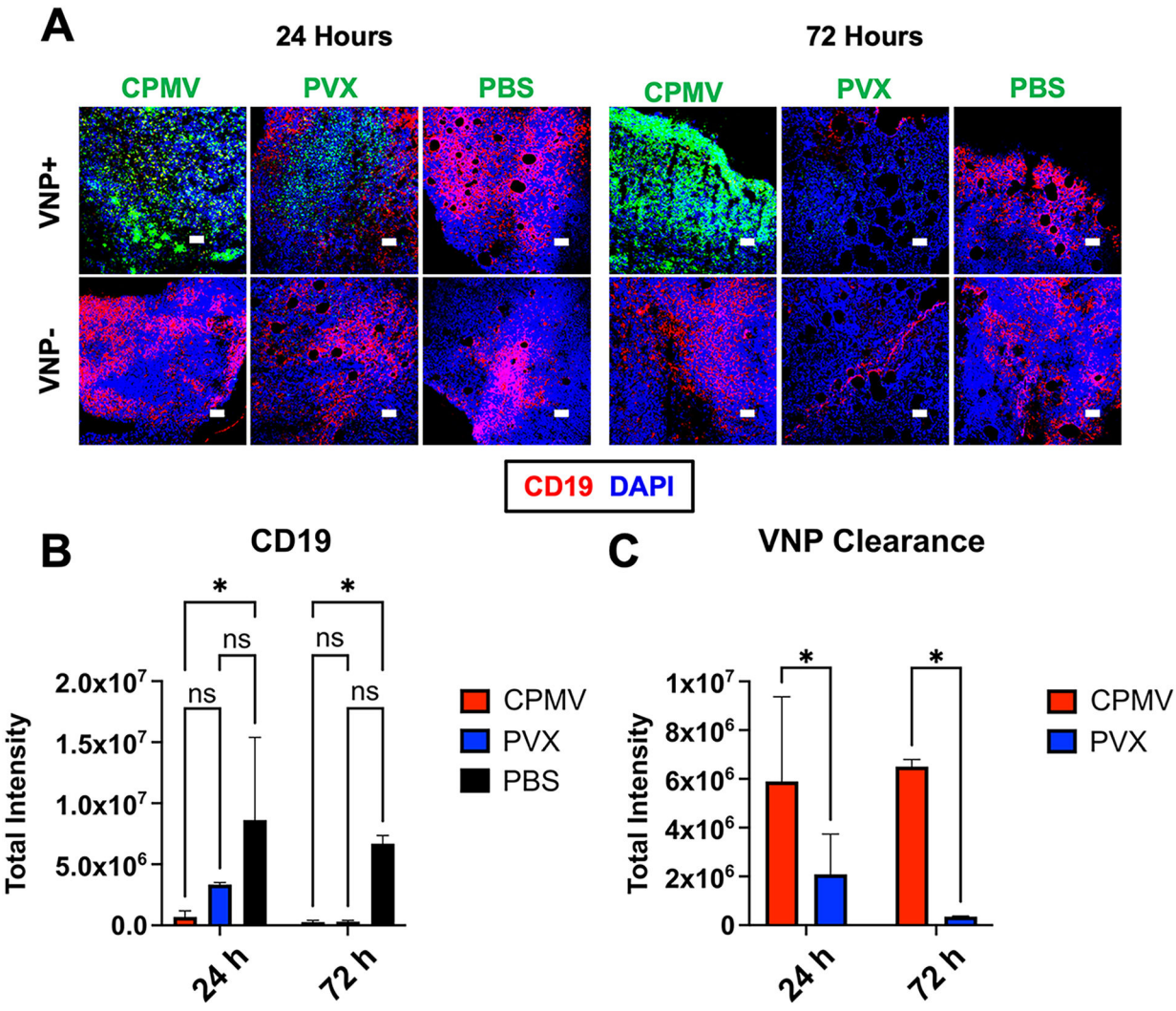

Figure 3.

Immunofluorescence imaging showing the clearance of B-cell lymphoma after intratumoral immunotherapy with CPMV or PVX. (A) Tumors were collected 24 and 72 h after the administration of CPMV or PVX as an intratumoral immunotherapy. The VNP+ regions of tumors (top row) show the depletion of CD19+ B cells 24 and 72 h after intratumoral immunotherapy, whereas the VNP—regions (bottom row) feature abundant CD19+ cells. After 72 h, PVX has been mostly cleared from the tumor whereas a large quantity of CPMV remains (top row). The CD19+ signal in the VNP—regions of the tumor (bottom row) are comparable to the PBS control. Scale bar = 50 μm. (B) Quantification of confocal images shows both CD19 and VNP clearance. PBS treated animals have increased CD19 signal corresponding to tumor cells. (C) CPMV signal is strong after 72 h with PVX being rapidly cleared from the tumors. Analysis was based on 2–3 images per staining, each data point corresponds to the total intensity from an individual image. Statistical analysis was performed using 2-way ANOVA-Tukey's multiple comparisons test (*$p < 0.05$) using GraphPad Prism v10.2.0 software.

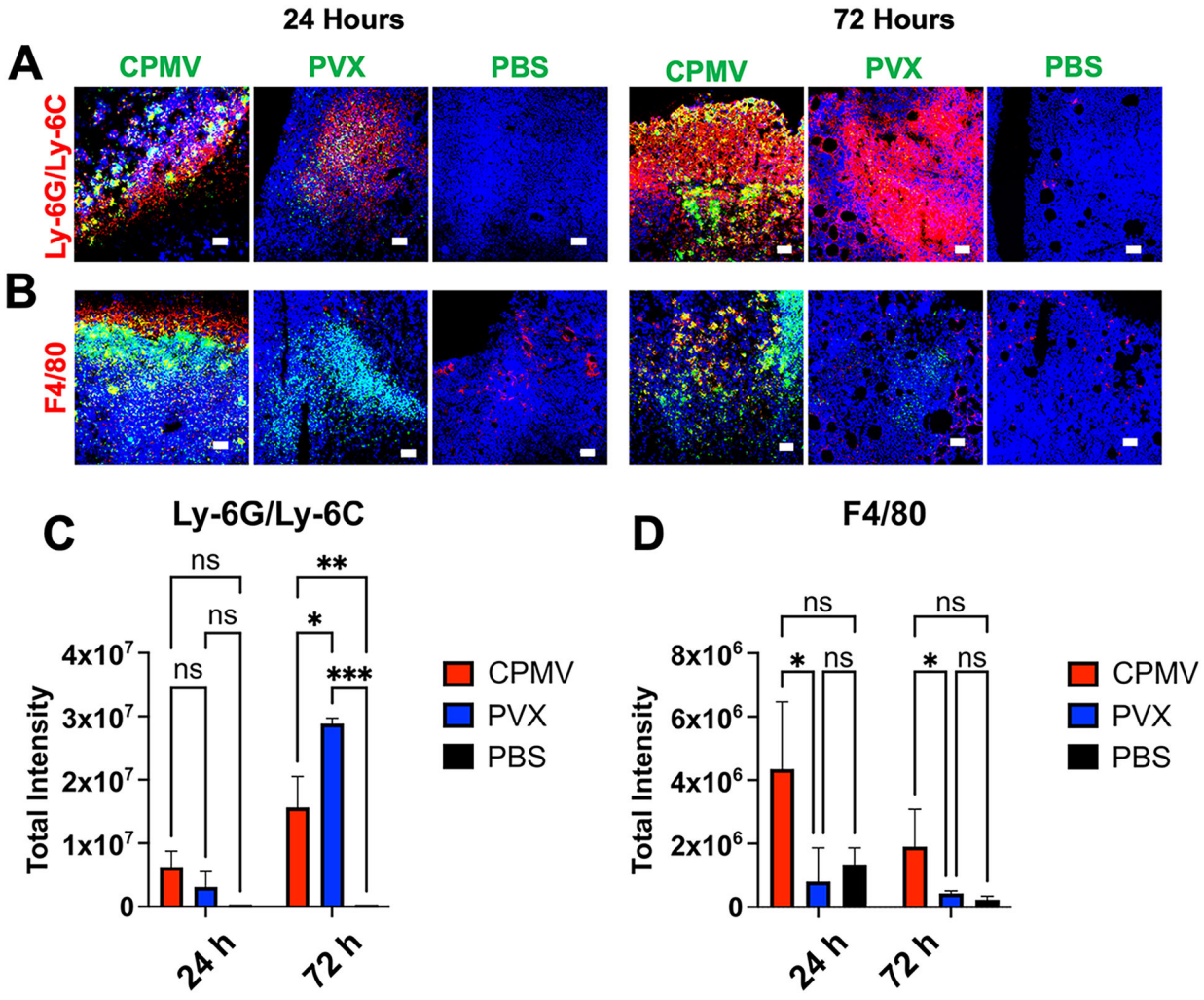

Figure 4.

Immunofluorescence imaging showing innate immune cell infiltration following intratumoral immunotherapy. (A) CPMV and PVX colocalize with tumor-infiltrating myeloid cells. PVX recruits myeloid cells with the same efficacy as CPMV despite the former's rapid clearance. (B) CPMV, but not PVX, is colocalized with tumor-infiltrating macrophages. DAPI was used for nuclear counterstaining (blue). Scale bar = 50 μm. Quantification of confocal images show immune cell infiltration into tumors. (C) Both CPMV and PVX lead to an increase in myeloid cell infiltration 72 h after intratumoral immunotherapy. (D) CPMV, but not PVX, leads to macrophage infiltration after intratumoral immunotherapy. Analysis was based on 2–3 images per staining, each data point corresponds to the total intensity from an individual image. Statistical analysis was performed using 2-way ANOVA–Tukey's multiple comparisons test (*$p < 0.05$, **$p < 0.01$, ***$p < 0.001$) using GraphPad Prism v10.2.0 software.

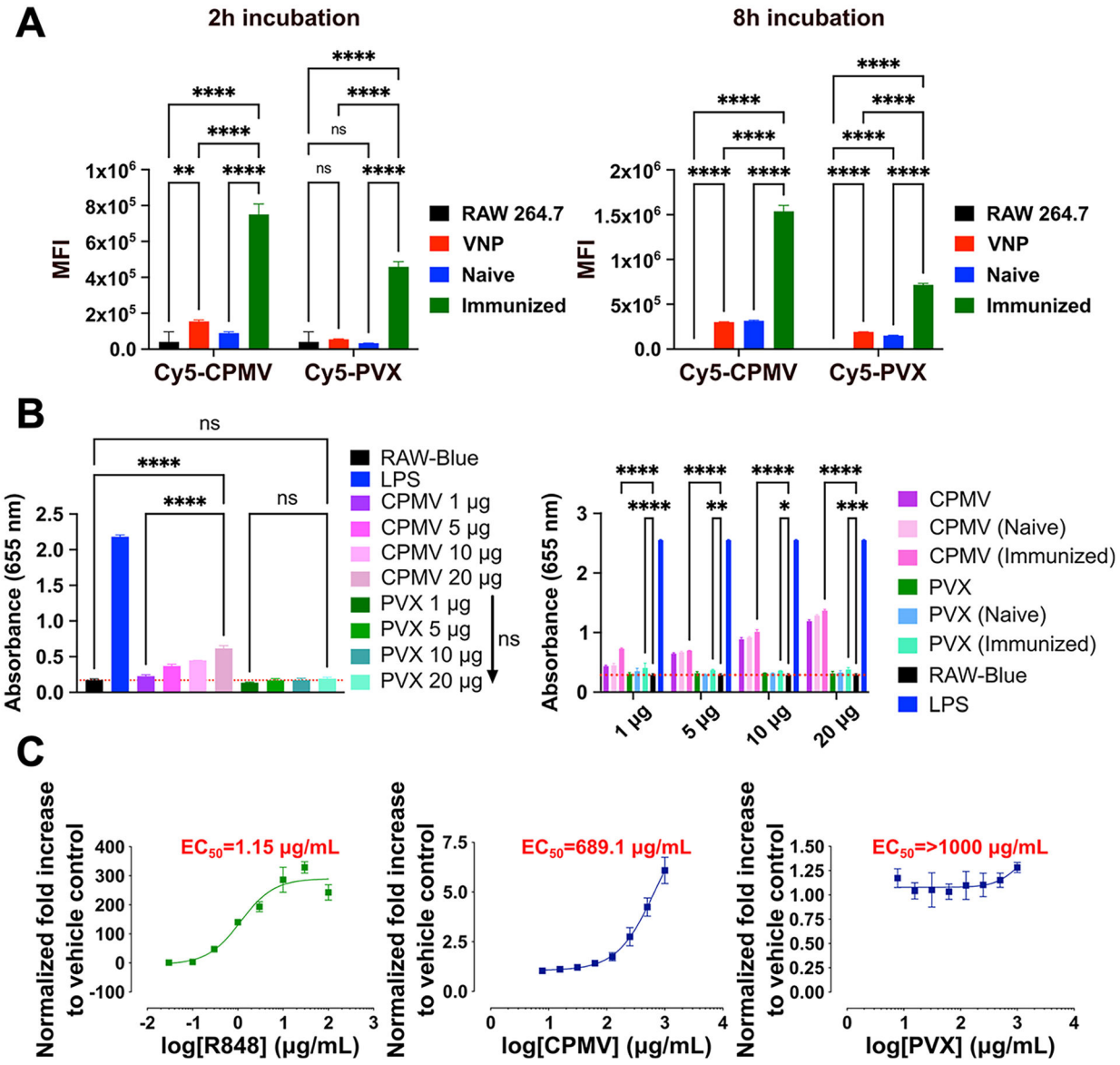

Figure 5.

Specific anti-VNPs antibodies enhanced CPMV and PVX uptake and immunogenicity. (A) Specific anti-CPMV and anti-PVX antibodies enhanced VNPs uptake over time. Cy5-CPMV or Cy5-PVX uptake by macrophages (RAW 264.7) was analyzed by flow cytometry in the presence (Immunized) and absence of immunized mice plasma (Naïve). Cy5-CPMV or Cy5-PVX (namely VNPs; 1 μg) were incubated with immunized or naïve mice plasma (1:200) prior to incubation with macrophages for 2 and 8 h (Figure S8). Statistical analysis was performed using 2-way ANOVA–Tukey's multiple comparisons test (****p < 0.0001) using GraphPad Prism v10.2.0 software. (B) Immunogenicity of CPMV and PVX was assessed by NF-κB/AP-1 activation in RAW-Blue cells in the presence and absence of specific anti-VNP antibodies. CPMV showed concentration-dependent NF-κB/AP-1 activation that was enhanced by the presence of anti-CPMV antibodies. For PVX, minimal activation was observed in the presence of anti-PVX antibodies. Statistical significance was

determined by one-way ANOVA with Tukey's multiple comparisons test (**$p = 0.018$, ****$p < 0.0001$; leftmost graph) or two-way ANOVA with Tukey's multiple comparisons test (*$p = 0.0276$, **$p = 0.024$, ***$p = 0.0002$, ****$p < 0.0001$; rightmost graph). (C) Half-maximal effective concentration (EC_{50}) of CPMV and PVX against TLR7 using a TLR7/NF-κB Luc reporter-HEK293 cell line. CPMV showed moderate TLR7 agonist activity (EC_{50} = 689 μg/mL) whereas PVX did not trigger TLR7 signaling (EC_{50} > 1000 μg/mL). The TLR assays were carried out by Abeomics Inc., CA, USA.